공학석사학위논문

Experimental Analysis of Local Flame Describing Function in a Model Rocket Combustor

모델 로켓 연소기에서의 국부 화염묘사함수에 대한 실험적 분석

2019 년 2 월

서울대학교 대학원

기계항공공학부

김 성 헌

Abstract

Experimental Analysis of Local Flame Describing Function in a Model Rocket Combustor

Seongheon Kim
School of Mechanical and Aerospace Engineering
The Graduate School
Seoul National University

In the development of liquid rocket engines, the transition to staged combustion cycle is being made. Among them, full-flow staged combustion cycle (FFSCC) is suitable for next generation of the rocket engines because it has longer engine life and higher reliability. Combustion instability phenomenon, which is considered a main obstacle in development of rocket engines, can lead to reduction of combustion efficiency and destruction of the combustion chamber in severe cases. Therefore, research to prevent such consequence is essential.

The purpose of this research is to recognize that spatial analysis is important when the length of the flame is long, such as rocket combustion. So instead of formerly used global flame transfer function (FTF) and flame describing function (FDF), in

this study, locally distributed FTF and FDF were measured using OH* chemiluminescence images and attempted to interpret the obtained functions in an experimental approach.

As a result, the perturbation of the heat release rate increased towards the flame tip, which affected the gain of local FTF and FDF. This could be explained by the interaction between flow and flame. Moreover, it was found that the nonlinear response of the flame became stronger towards the flame tip through the measurement of local FDF. It was confirmed that the gain tendency of the local FDF was related to the characteristic length of the flame.

Based on these results, it can be said that spatially obtained FTF and FDF may better reflect the flame response while used to predict combustion instability, when the flame is long as rocket flame.

Keywords : combustion instability, local flame describing function, local flame transfer function, local heat release rate, model rocket combustor, swirl-jet coaxial injector, velocity fluctuation, flame length

Student Number : 2016-20729

CONTENTS

LIST OF FIGURES

LIST OF TABLES

NOMENCLATURE

w	frequency
q'	heat release rate fluctuation
$\bar{q}$	mean heat release rate
u'	inlet velocity fluctuation
$\bar{u}$	inlet mean velocity
$\|u'\|$	inlet velocity fluctuation amplitude
FTF	flame transfer function
FDF	flame describing function
FFT	fast Fourier transform
HWA	hot wire anemometer
PIV	particle image velocimetry
SLPM	standard liter per minute

CHAPTER 1

INTRODUCTION

1.1. Full-Flow Staged Combustion Cycle

Although engineering complexity is a demerit for staged combustion cycle (SCC) in rocket engines, its advantages are significant that it is applied to various engines nowadays. In Korea, the development of SCC rocket engine has been conducted since 2006 and it is now in the phase of testing technology demonstration model [1].

As it is known that there are several variants for SCC, full-flow staged combustion cycle (FFSCC) is the one with numerous benefits. FFSCC, as shown in Fig. 1.1, the cycle uses both propellants fully to operate fuel and oxidizer turbopumps respectively. Its advantages, which are longer engine life and higher reliability, can be achieved by turbines that are operated at lower pressure and temperature [2,3]. Moreover, FFSCC can be operated without an interpropellant turbine seal to separate oxidizer-rich gas from the fuel turbopump or fuel-rich gas from the oxidizer turbopump, which results in improved reliability. FFSCC has a distinct feature which is full gasification of both propellants before entering the main combustion chamber. This leads to rapid chemical reactions in the chamber, which boosts the performance

of the engine [4]. Hence, FFSCC is suitable for the next generation of rocket engines and should be the target of development.

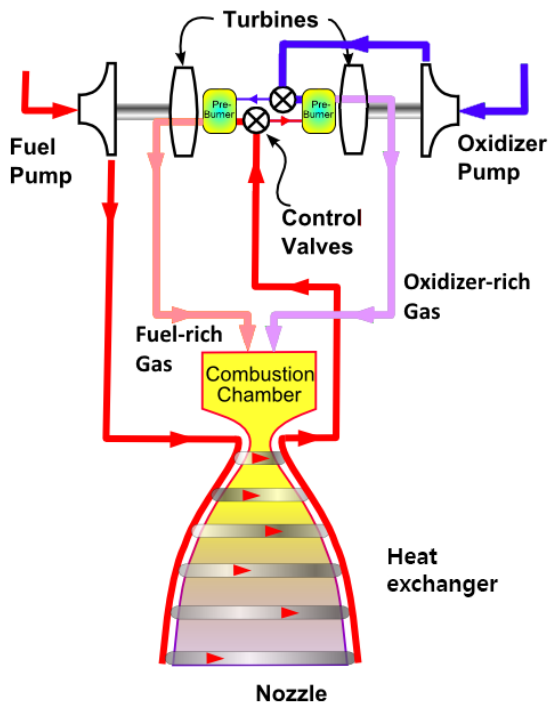

Fig. 1.1 Schematic diagram of full-flow staged combustion cycle

1.2. Combustion Instability

Combustion instability phenomenon, which occurs in the combustion chamber, was always an obstacle in development of rocket engines. This phenomenon hinders the combustion efficiency and in severe cases, it can lead to failure of the whole engine system. Thus, it is important to predict and avoid this circumstance while the engine is running.

As shown in Fig. 1.2, combustion instability is caused by feedback loop of three kinds of oscillations: flow rate, heat release rate, and acoustics [5]. Since combustion instability is a complicated phenomenon, there were endeavors to interpret in a decomposed manner.

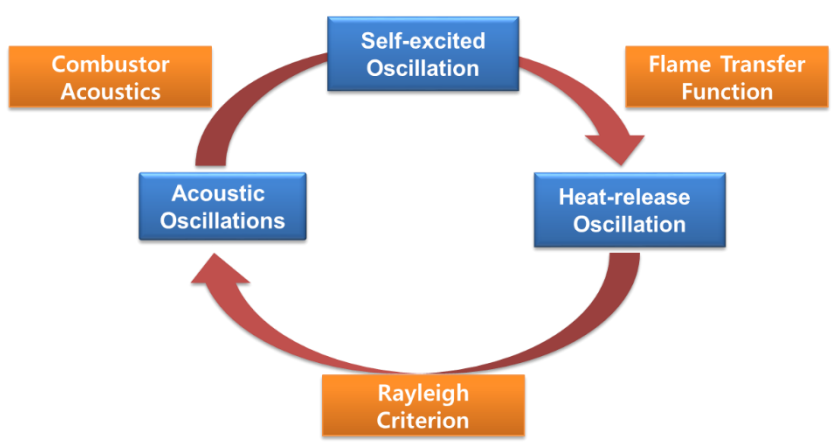

Fig. 1.2 Mechanism of combustion instability

The relationship between flow velocity oscillation and heat release rate perturbation can be represented by flame transfer function (FTF) which is expressed as follows:

$$\mathrm{FTF(w)} = \frac{q'/\bar{q}}{u'/\bar{u}} \qquad \text{Eq. 1}$$

FTF can be attained by various methods including experimental [6-8], computational [9,10], and analytical [11-13]. It is used as an input to determine the eigenfrequency and growth rate of a low-order thermo-acoustic system model. However, FTF cannot be used to predict the limit cycle amplitude, since the limit cycle amplitudes are governed by nonlinear effects. To resolve these nonlinear effects, so-called flame describing function (FDF) came up and it can be expressed by Eq. 2 [14].

$$\mathrm{FDF(w}, |u'|) = \frac{q'/\bar{q}}{u'/\bar{u}} \qquad \text{Eq. 2}$$

FDF can not only estimate limit cycle amplitudes and frequencies but also interpret various nonlinear features manifested in practical systems such as mode switching, nonlinear triggering, and frequency shifting [15].

1.3. Research Objectives

Although there are numerous studies done on FTF and FDF because of their importance in combustion instability, not much researches regarded locally defined FTF or FDF. For flames that are not acoustically compact, acoustic wave and heat release wave have similar length scale, which means satisfaction of the Rayleigh criterion could be varied by region. Fig. 1.3 shows an example of rocket combustion which is not acoustically compact [16].

Acknowledging the importance of spatial analysis in rocket combustion, experimental measurement and analysis of local FTF and FDF was conducted in a model rocket combustor with single swirl-jet coaxial injector. In addition, the effect of flow field and flame length on local FTF and FDF was determined.

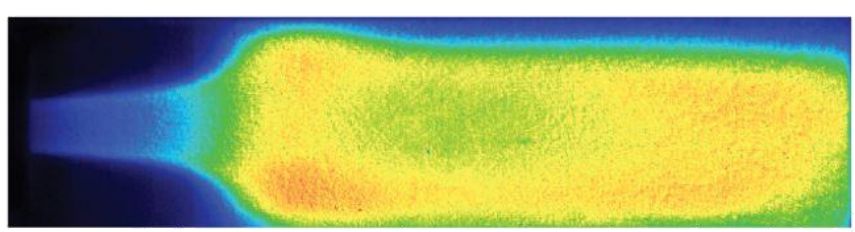

Fig. 1.3 OH* chemiluminescence image of LOX/GCH_4 flame in high pressure rocket engine combustor

CHAPTER 2

EXPERIMENTAL APPARATUS AND METHOD

2.1. Experimental Apparatus and Method

Schematic of closed boundary model rocket combustor and the injector used in this study are shown in Fig. 2.1 and Fig. 2.2 respectively.

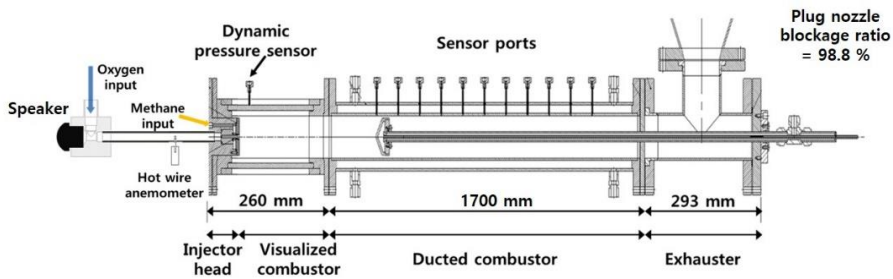

Fig. 2.1 Schematic diagram of closed boundary model rocket combustor

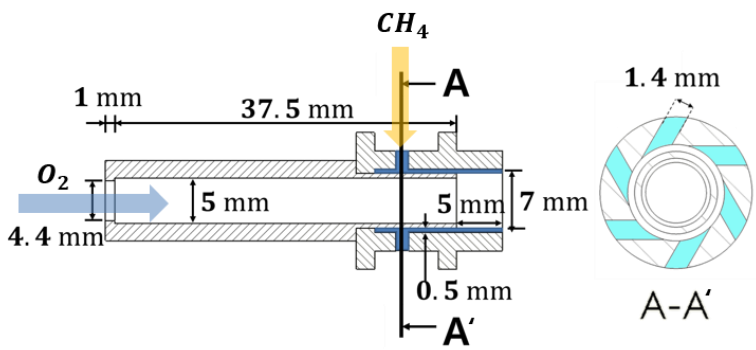

Fig. 2.2 Schematic diagram of swirl-jet coaxial injector

Quartz window facilitates visualization of the flame and acoustic boundary can be adjusted by the plug nozzle which has blockage ratio of 98%. The injector design is similar to that of gas centered swirl coaxial injector used in RD-8 and RD-170 engines. Gas state of oxidizer is supplied in the center by jet and the fuel enters in circumferential direction so that it can generate swirl effect. In real engines, liquid kerosene was used as fuel, but for FFSCC, gas state of fuel should enter the main combustion chamber. Also, as methane is spotlighted as an environment-friendly fuel and is used in reusable launch vehicle recently, gas state of methane was selected in this research.

As FTF and FDF concern only the relationship between velocity perturbation and heat release rate oscillation, acoustic effect, which can generate self-excited instability, should be excluded. In order to eliminate the acoustics inside the combustion chamber, the rear part of the combustor was removed as shown in Fig. 2.3. Flow velocity fluctuation, which is the denominator of the functions, is made by perturbing the oxidizer with a speaker.

Frequency range of the speaker is up to 1000 Hz. The amplitude of the velocity fluctuation was measured by hot wire anemometer (HWA) (Dantec, MiniCTA) which is located ahead of the injector. Heat release rate fluctuation from the flame,

denominator of the functions, was measured using OH* chemiluminescence images taken by high-speed CMOS camera (LaVision HighSpeedStar 8) aided with intensifier (HighSpeed IRO). Spatial resolution was 1024 × 512 pixels and UV lens (100 mm, f 2.8) and filter (bandpass filter, 308 ± 10 nm) was used.

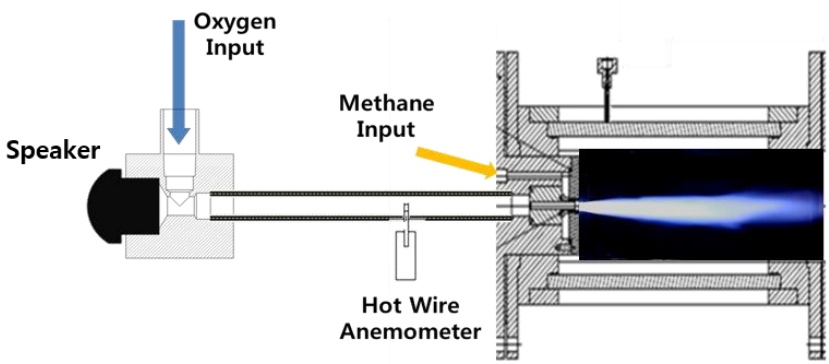

Fig. 2.3 Open boundary combustor for FTF and FDF measurement

Details of heat release rate measurement are explained below. In this study, heat release rate was represented by OH* chemiluminescence intensity which is calculated by image processing. In order to relate heat release rate with OH* chemiluminescence intensity, there should be a coherent connection when the equivalence ratio is altered.

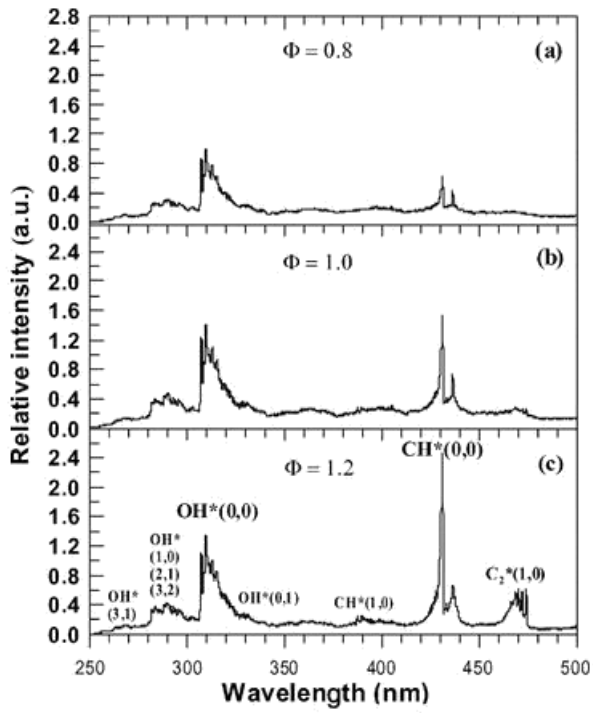

Fig. 2.4 Relative intensity of OH* chemiluminescence for various equivalence ratio

Cheng et al. found that in partially premixed methane flame, OH* chemiluminescence intensity increases with equivalence ratio from 0.8 to 1.2 as it is shown in Fig. 2.4 [17].

Presented in Fig. 2.5, for local heat release rate calculation, image was divided into 10 regions and denominated the closest region to the injector as flame base, the farthest region as flame tip, and in-between as middle part of the flame. The flame

base area was selected slightly apart from the injector in order to employ meaningful value of the fluctuation. Images were taken at 7k Hz sampling rate and 7000 images were used to calculate heat release rate for each cases.

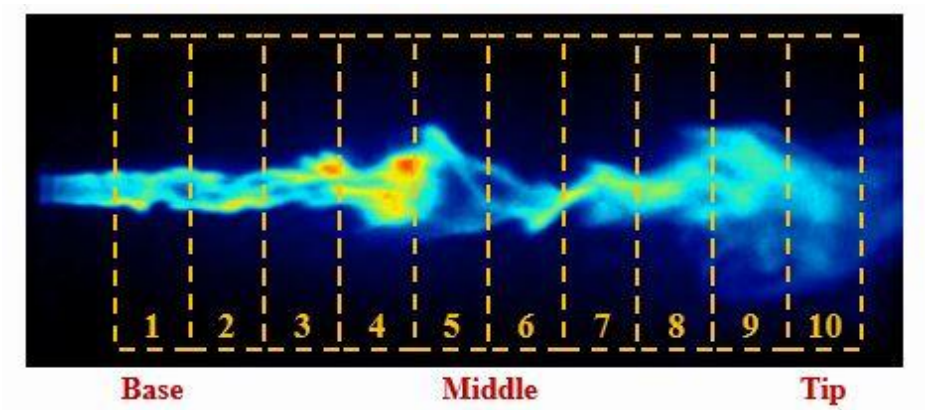

Fig. 2.5 10 divided regions for calculating OH* chemiluminescence intensity

The heat release fluctuation calculation was utilized by MATLAB. First, the images were converted to gray scale by LaVision program. Then the gray scale images were taken into MATLAB. For each selected regions, summation of the intensity was carried out. For global heat release, all 10 regions were summed. Finally, fast Fourier transform (FFT) was conducted to find out the fluctuation value at the excited frequency.

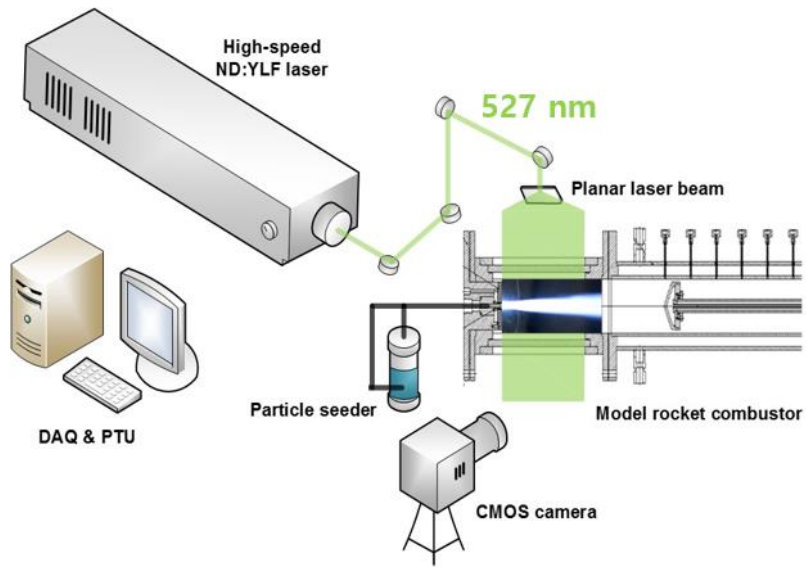

Fig. 2.6 PIV measurement settings

To analyze the results of FTF and FDF, particle image velocimetry (PIV), was conducted to examine the effect of flow field inside the combustor chamber. PIV measurement settings are presented in Fig. 2.4. Nd:YLF double pulse laser (Photonics, DM20-527) with wavelength of 527 nm was used and sheet optics were applied to render planar laser beam. CMOS camera used for PIV was the same with measurement for OH* chemiluminescence. Size of under 100 μm ZrO_2 was the seeding particle and the filter (bandpass filter, 532 ± 10 nm) enabled signals from the particles to be detected by camera.

2.2. Experimental Conditions

Before conducting FTF and FDF measurement, closed boundary combustion instability test was done to select cases for the research. As shown in Fig. 2.7, 1L mode instability amplitude differed by fuel flow rate and equivalence ratio at combustor length of 1560 mm. Instability amplitude increased with higher fuel flow rate and had up-and-downs with increasing equivalence ratio. To identify the effect of fuel flow rate, at equivalence ratio 1.0, case 1 and 2 were chosen which have fuel flow rate of 20 SLPM and 45 SLPM respectively. To confirm the effect of equivalence ratio difference, case 3 was chosen at equivalence ratio of 1.25 with same methane flow rate as case 2. Equivalence ratio of 1.25 was selected because it is the approximate value used in real rocket engines.

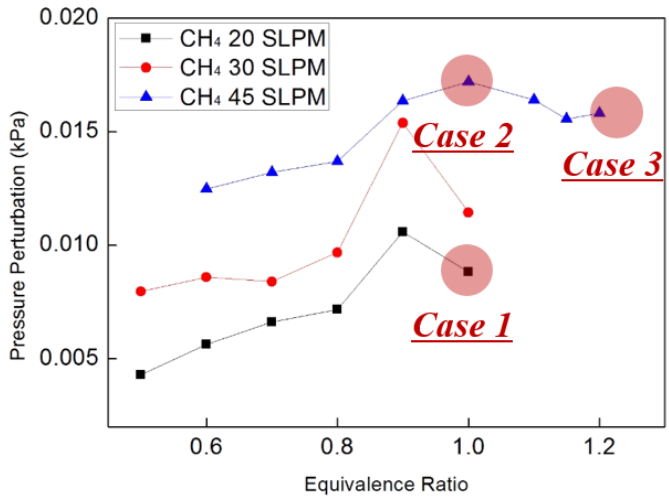

Fig. 2.7 Closed boundary combustion instability characteristics and selection of cases for local FDF measurement

Table. 2.1 Experimental conditions

Local FDF Test Condition	
Fuel & Oxidizer	**CH_4 & O_2 (Gas)**
Fuel Flow Rate	**20, 45 SLPM**
Equivalence Ratio	**1.0, 1.25**
Input Fluctuation Frequency	**50 ~ 500 Hz (10 or 50 Hz step)**
Input Fluctuation Amplitude	**0.1, 0.2, 0.3**
Inlet Pressure	**Ambient**
Inlet Temperature	**25 ℃**

Table. 2.1 shows the details of experimental conditions. Gas state of methane and oxygen were used. Fuel flow rate and equivalence ratio information is mentioned when selecting 3 cases. Excitation frequency range was 50 ~ 500 Hz by 10 or 50 Hz steps. For FDF measurement, 3 kinds of frequency modulation amplitude was chosen: 0.1, 0.2, and 0.3. Inlet pressure and temperature were at ambient.

CHAPTER 3

RESULTS AND DISCUSSIONS

3.1. Global Flame Describing Function

Before investigating local FTF and FDF, global FDF results were examined. Fig. 2.8 shows the global FDF result of case 1 (in order of gain, phase, delay time from the top). Almost the same tendency was found in gain graph. The only difference was found at frequency of 200 Hz which indicates nonlinear response of the flame.

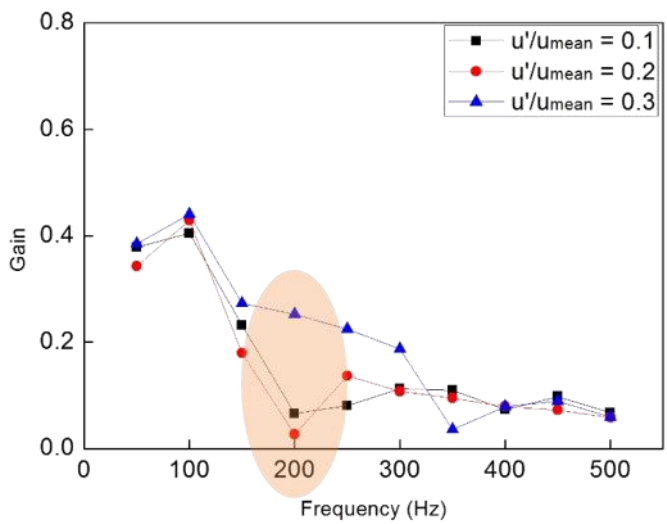

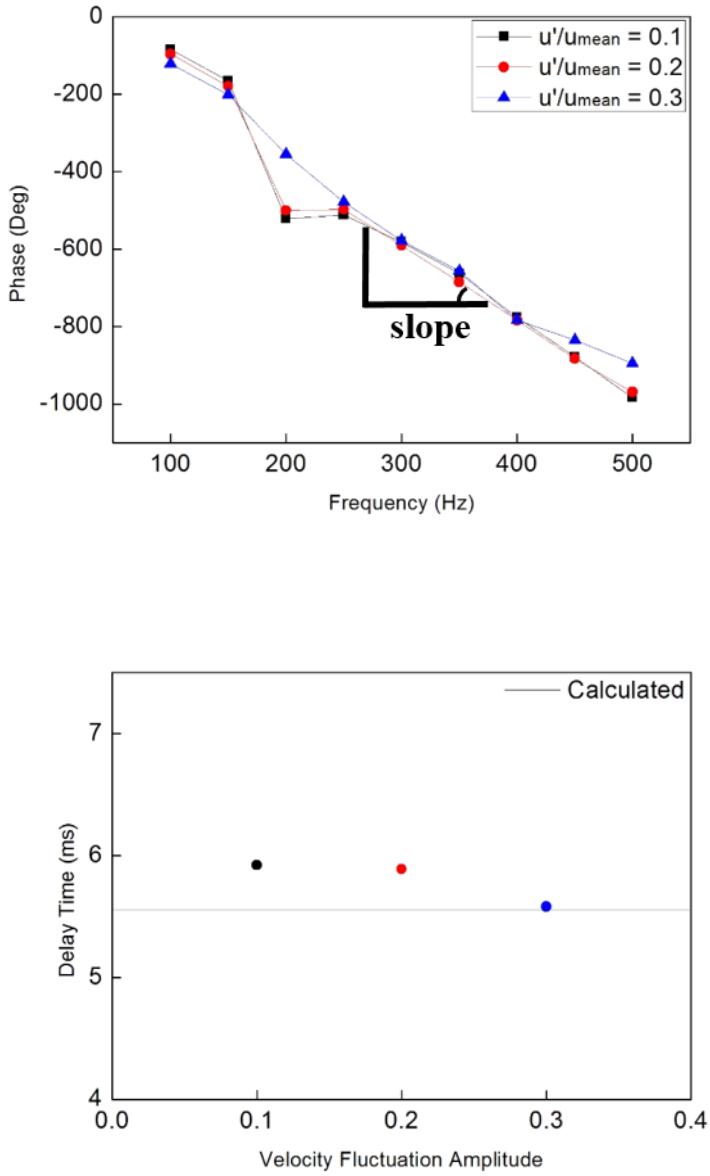

Fig. 3.1 Global FDF result of case 1: 20 SLPM, Eq 1.0 (in order of gain, phase, delay time from the top)

Phase graph also showed similar trends at different modulation amplitudes. Utilizing the slope of the phase, delay time could be calculated by the equation follows:

$$Delay\ time = \frac{phase\ slope}{360°} \qquad \text{Eq. 3}$$

The black horizontal line in the delay time graph indicates the delay time calculated using effective flame length and the theoretical exit jet velocity. It can be expressed by Eq. 4. Effective flame length is the length between the flame front and the maximum point of OH* chemiluminescence intensity.

$$Calculated\ delay\ time = \frac{effective\ flame\ length}{exit\ jet\ velocity} \qquad \text{Eq. 4}$$

Delay time calculated using the phase slope was slightly higher because the real exit jet velocity should be reduced by diffusion effect when it passes through the injector.

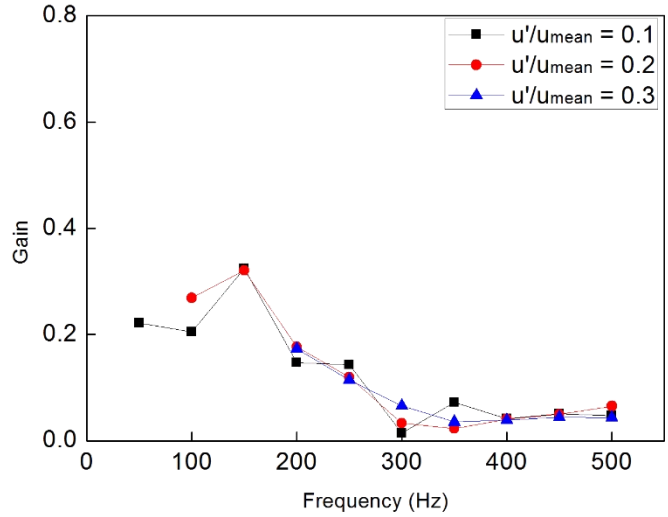
0.8
0.6
0.4
0.2
0.0
Gain
0
100
200
300
400
500
Frequency (Hz)
u'/umean = 0.1
u'/umean = 0.2
u'/umean = 0.3

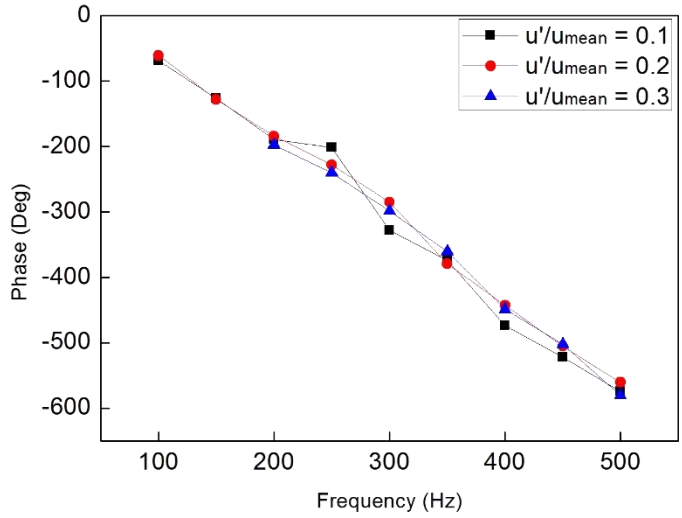
0
-100
-200
-300
-400
-500
-600
Phase (Deg)
100
200
300
400
500
Frequency (Hz)
u'/umean = 0.1
u'/umean = 0.2
u'/umean = 0.3

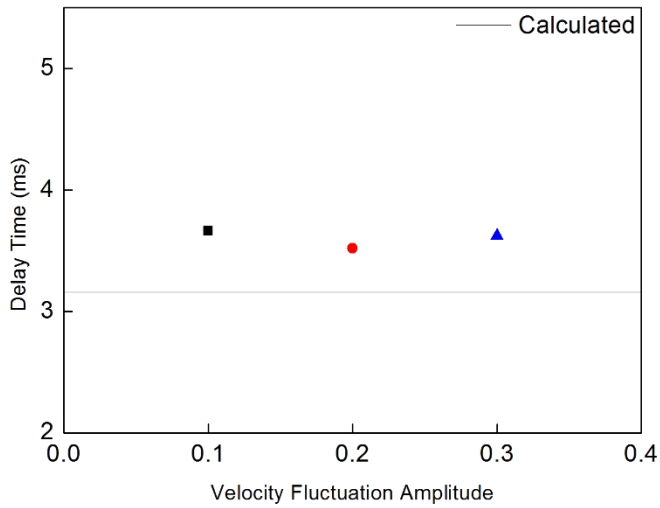

Fig. 3.2 Global FDF result of case 2: 45 SLPM, Eq 1.0 (in order of gain, phase, delay time from the top)

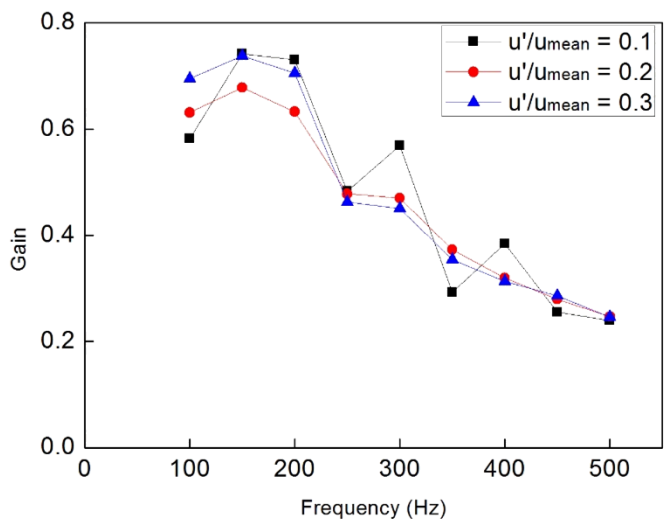

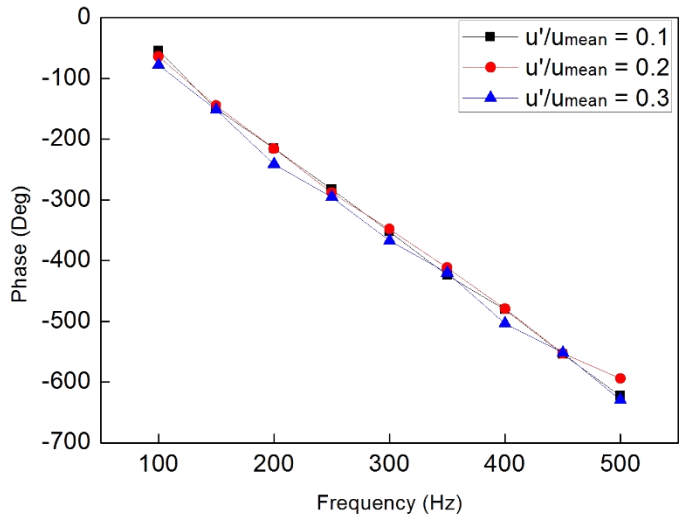

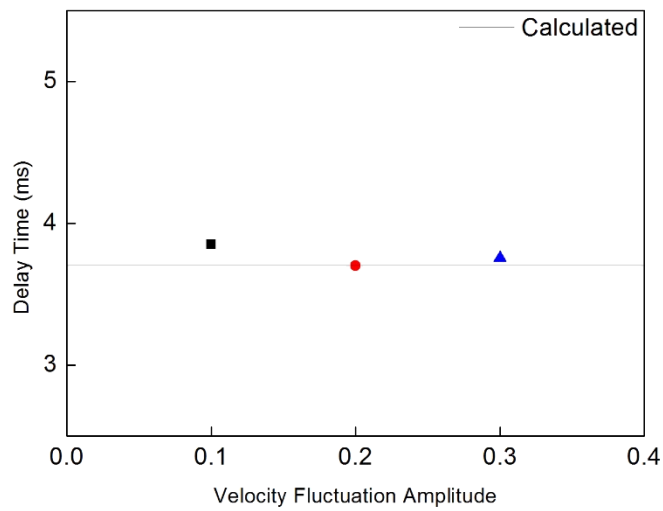

Fig. 3.3 Global FDF result of case 3: 45 SLPM, Eq 1.25 (in order of gain, phase, delay time from the top)

There was no distinct difference in gain graphs varied by fluctuation amplitudes for higher fuel flow rate cases as shown in Fig. 3.2 and 3.3. However, the peak frequency was moved to near 150 Hz and for same fuel flow rate, higher equivalence ratio had higher gain tendency. Phase trends were almost equivalent. Higher fuel flow rate resulted in higher velocity which decreases the delay time. The difference between case 2 and case 3 in delay time was the result of oxygen flow rate. As the equivalence ratio was matched by oxygen flow rate, case 3 had lower oxygen flow rate which means it had lower velocity that influenced the delay time to be slightly higher.

3.2. Local Flame Transfer Function

3.2.1. Local Heat Release Rate

From now on, local analysis will be dealt with. As it can be seen from Fig. 3.4, normalized local heat release rate tended to increase from flame base to the flame tip region. In addition, this tendency maintained and also the normalized heat release rate increased when the fluctuation amplitude increased as shown in Fig. 3.5.

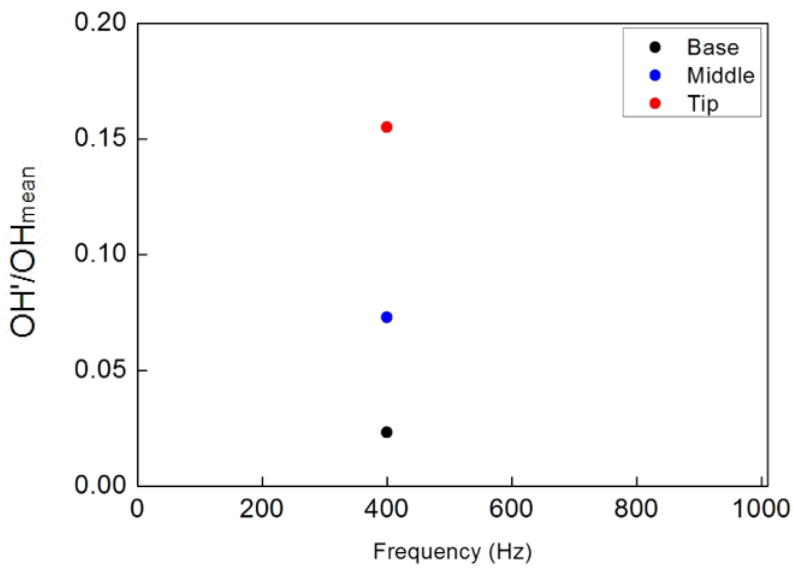

Fig. 3.4 FFT result of OH* chemiluminescence intensity of case 3: 45 SLPM, Eq 1.25, $u'/\bar{u} = 0.1$, 400 Hz excitation

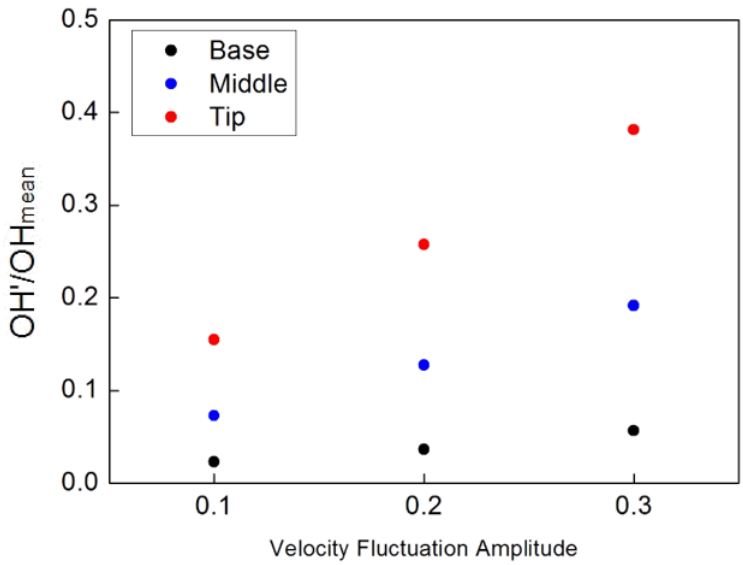

Fig. 3.5 FFT result of OH* chemiluminescence intensity of case 3: 45 SLPM,

Eq 1.25, $u'/\bar{u} = 0.1, 0.2, 0.3$, 400 Hz excitation

3.2.2. Local Flame Transfer Function Results

Based on the local heat release rate, local FTF was calculated using MATLAB. Local FTF gain increased and the slope of phase was steeper when the region of interest moved towards the downstream. Compared with the result from Kim et al.'s work as shown in Fig. 3.7, the tendency of the gain and phase was the same [18]. This indicates that using photomultiplier tube and camera to detect OH* chemiluminescence intensity lead to reasonably equivalent results.

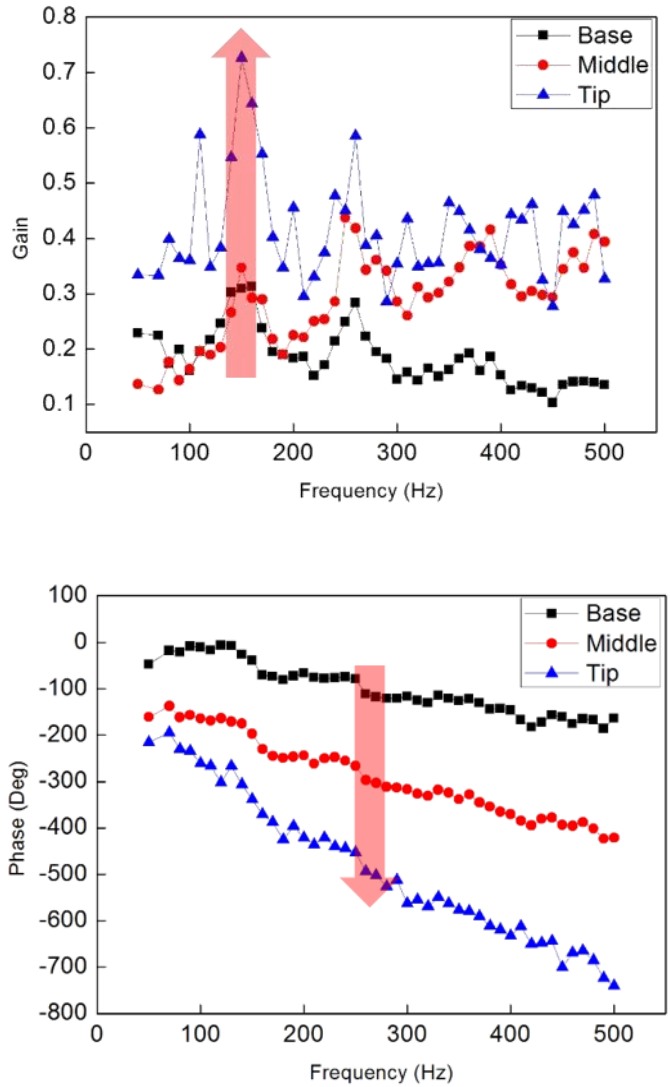

Fig. 3.6 Local FTF result of case 2: 45 SLPM, Eq 1.0, $u'/\bar{u} = 0.1$ (in order of gain, phase from the top)

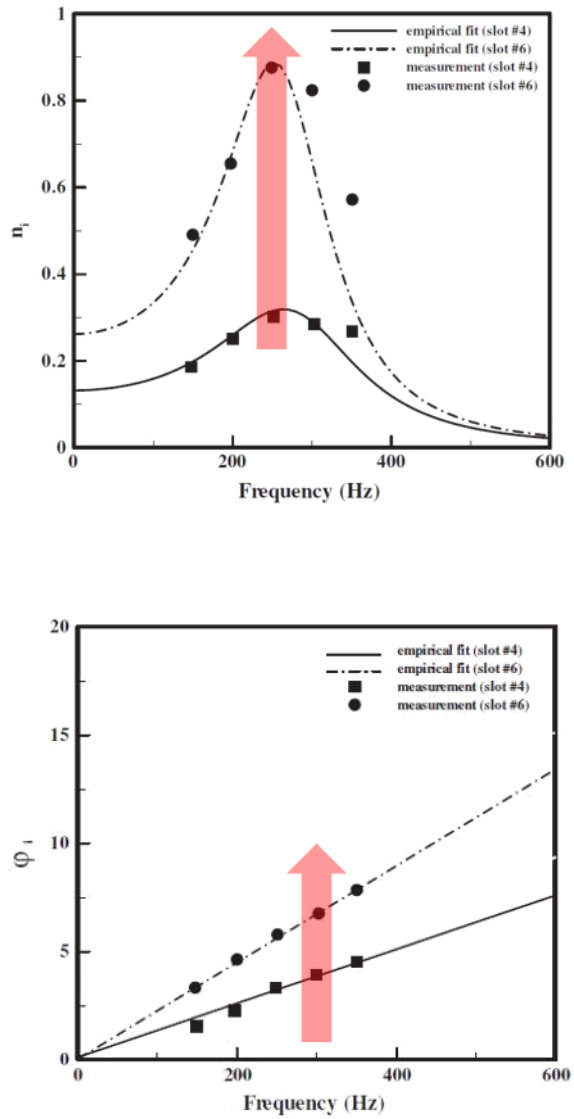

Fig. 3.7 Local FTF result from a previous study (in order of gain, phase from the top)

Case 3 showed similar trends of local FTF as case 2 as it is shown in Fig. 3.8. The starting degree of the phase graph decreased towards the flame tip. This is because theoretically, the degree at 0 Hz (no modulation) should be 0°. Then the steeper slope would have lower degree at 50 Hz which results as the phase graph of local FTF. Moreover, as mentioned at Eq. 3, steeper slope resulted in longer delay time which is obvious that it would take longer time to propagate towards the downstream. The global delay time was closest to the delay time of flame tip because the effective flame length is near the flame tip.

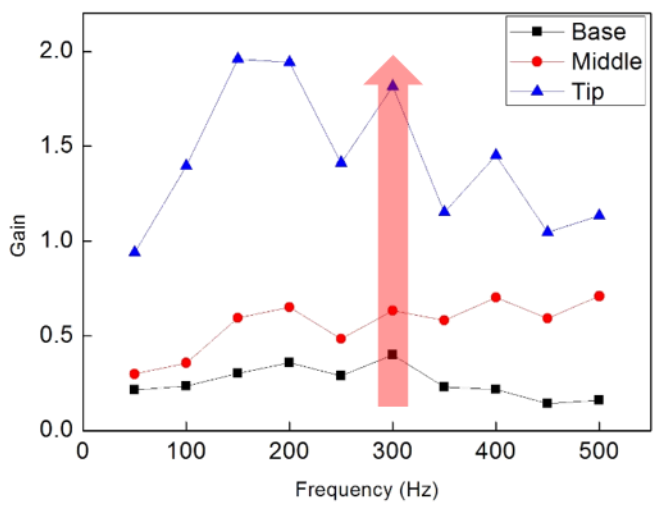

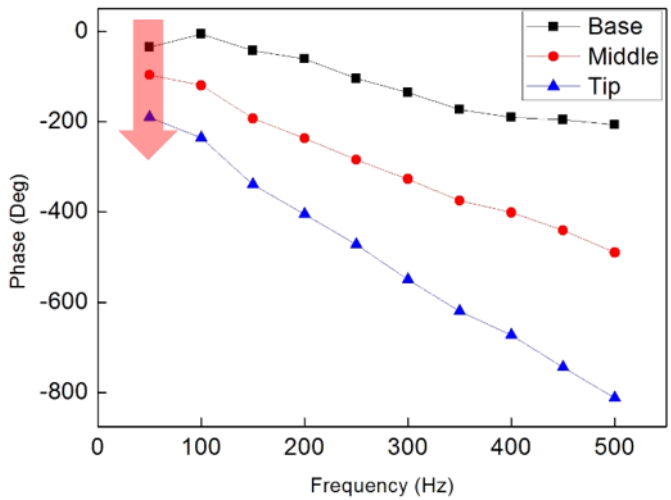

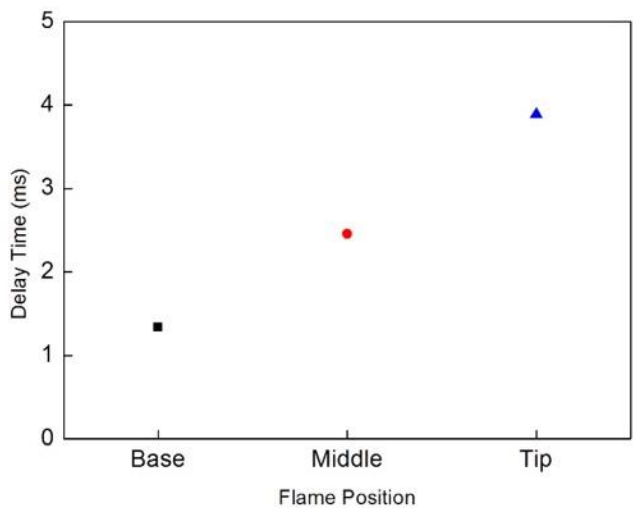

Fig. 3.8 Local FTF result of case 3: 45 SLPM, Eq 1.25, $u'/\bar{u} = 0.1$ (in order of gain, phase, delay time from the top)

3.2.3. Effect of Flow Field

In order to analyze the results of local FTF, PIV measurement was conducted. As it is shown in Fig. 3.9, 3 horizontal lines were chosen and the velocity profiles of them were extracted from PIV results. Then, selected 3 points that represented the flame base, middle, and tip area at the velocity profile data as it is presented in Fig. 3.10. 1000 data sets were used to calculate FFT using MATLAB in order to obtain velocity fluctuation amplitude measured by PIV.

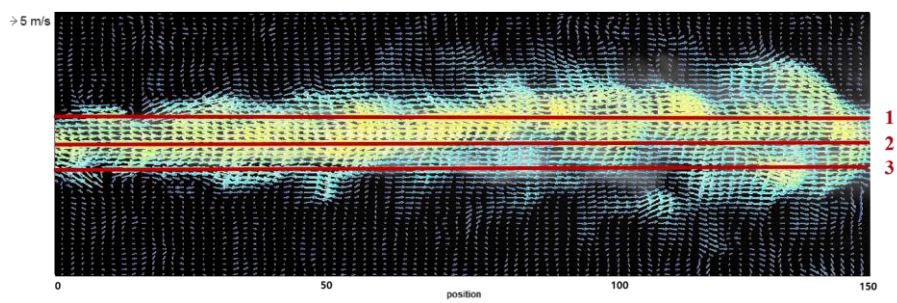

Fig. 3.9 Extraction of velocity profiles along the 3 horizontal lines

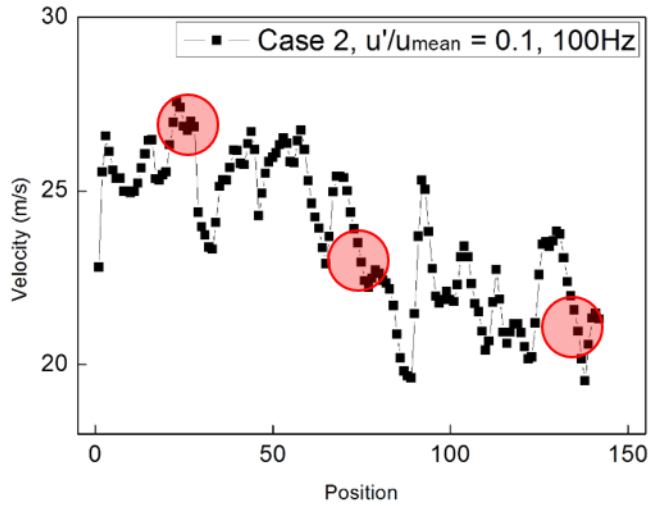

Fig. 3.10 Location of flame base, middle, and tip in velocity profile data

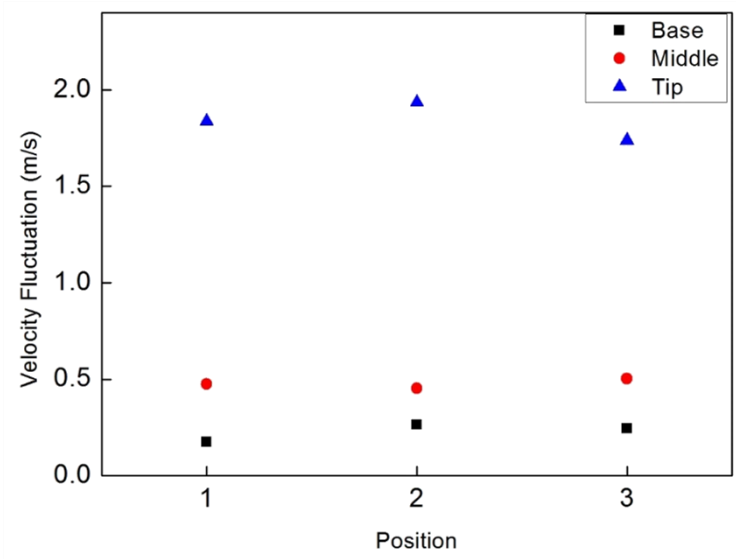

Fig. 3.11 Velocity fluctuation result of case 1: 20 SLPM, Eq 1.0, $u'/\bar{u} = 0.1$,

100 Hz excitation

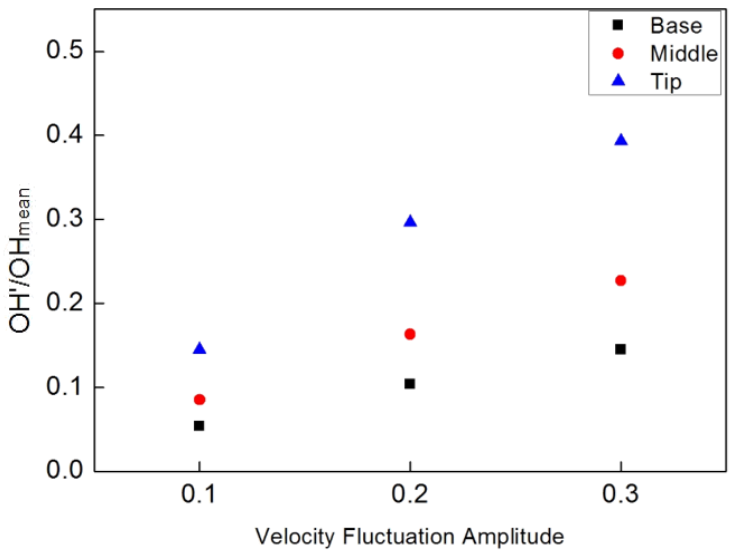

Fig. 3.12 Normalized OH* chemiluminescence intensity varied by velocity fluctuation amplitudes of case 1: 20 SLPM, Eq 1.0, 100 Hz excitation

As it can be noticed by Fig. 3.11, for all 3 horizontal lines, velocity perturbation magnitude increased towards the flame tip. For the same case, Fig. 3.12 shows that normalized OH* chemiluminescence intensities have higher value towards the flame tip also. This trend was sustained while the velocity perturbation amplitude increased. Due to these results, it can be said that flow fluctuation influenced the heat release rate as well as the gain of local FTF, which had coherent trends of growth towards the flame tip.

3.3. Local Flame Describing Function

3.3.1. Local Flame Describing Function Results

In this chapter, local FDF results will be presented. For case 1, as it is shown in Fig. 3.13, nonlinear response of the flame appeared from the middle region of the flame. If the flame response is linear, the gain value for all 3 velocity perturbation magnitudes should be the same. For the same region of interest, phase difference were not significant for various fluctuation amplitudes. But the slope of the phase, which has influence in the delay time, had the same tendency found in local FTF results.

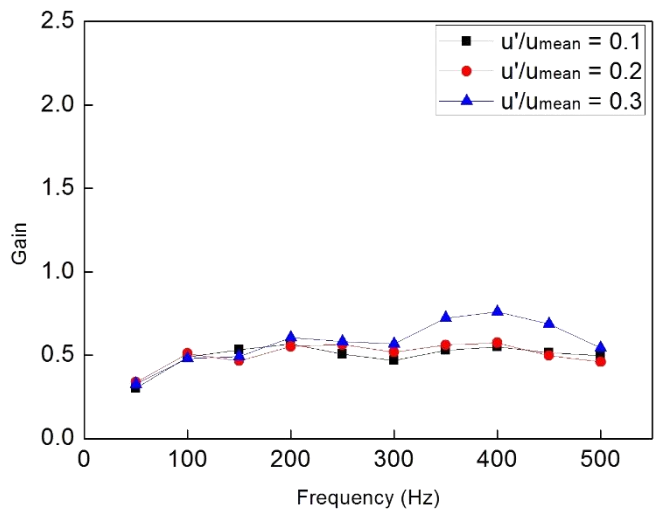

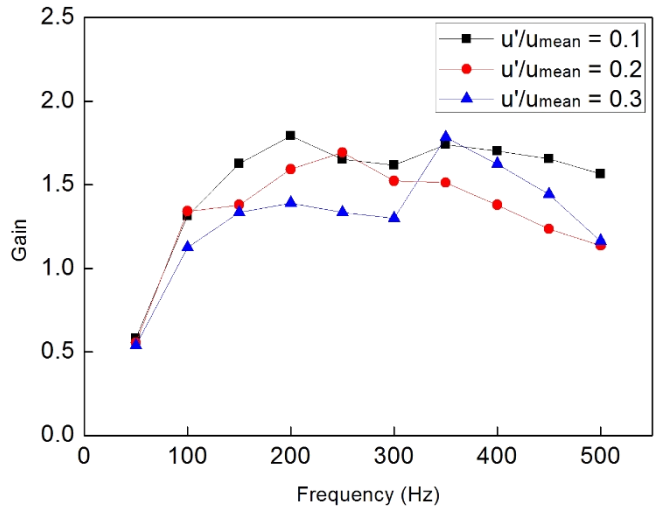

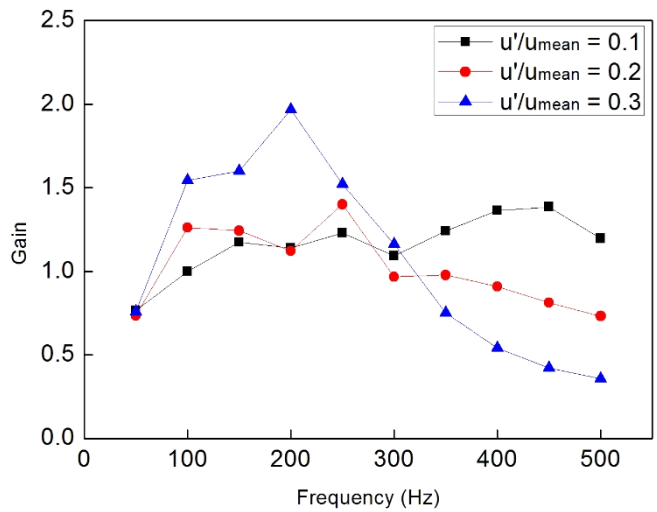

Fig. 3.13 Local FDF gain results of case 1: 20 SLPM, Eq 1.0 (in order of flame base, middle, and tip from the top)

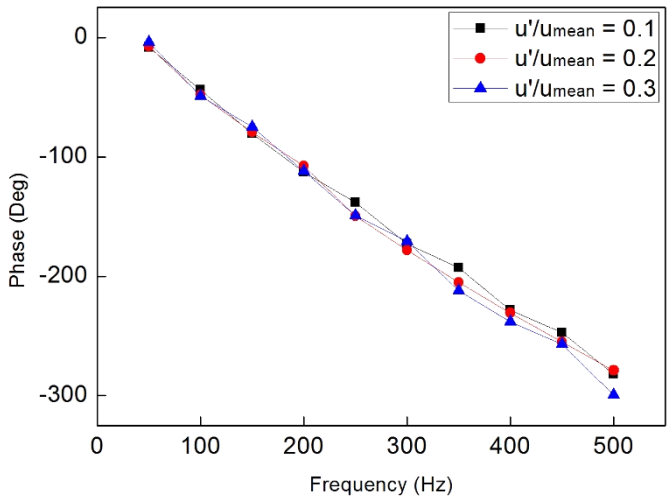
u'/umean = 0.1
u'/umean = 0.2
u'/umean = 0.3
Phase (Deg)
Frequency (Hz)
0
-100
-200
-300
0
100
200
300
400
500

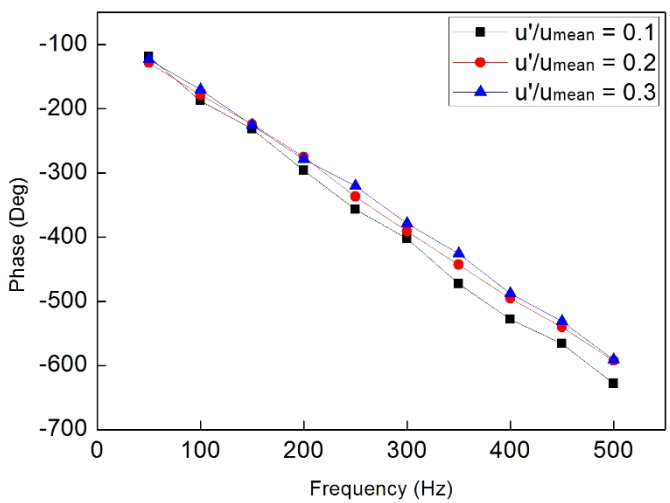
u'/umean = 0.1
u'/umean = 0.2
u'/umean = 0.3
Phase (Deg)
Frequency (Hz)
-100
-200
-300
-400
-500
-600
-700
0
100
200
300
400
500

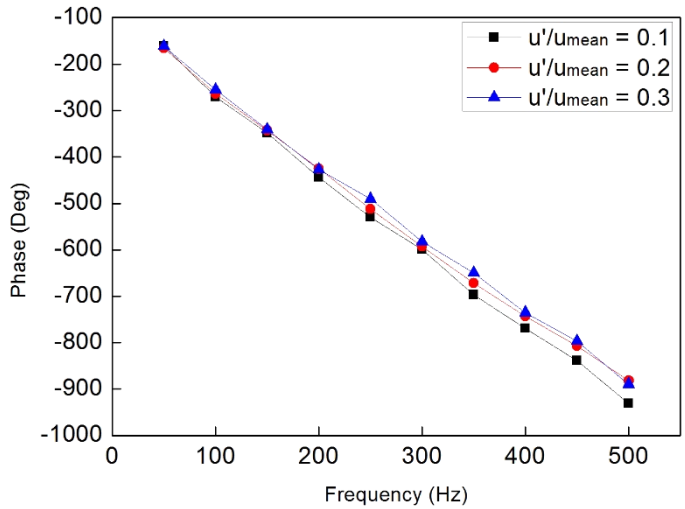

Fig. 3.14 Local FDF phase results of case 1: 20 SLPM, Eq 1.0 (in order of flame base, middle, and tip from the top)

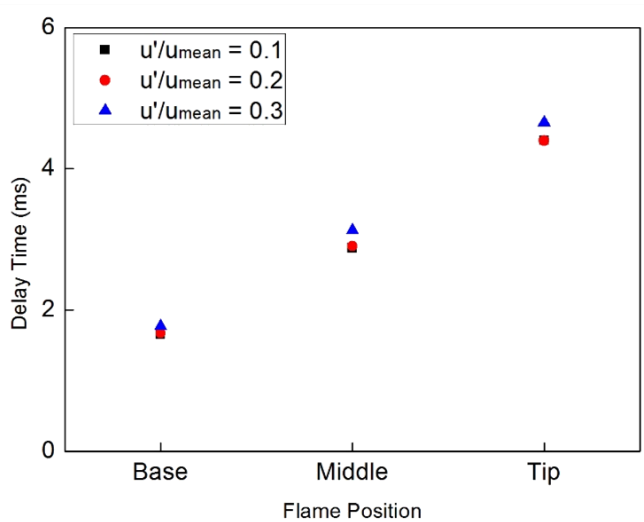

Fig. 3.15 Local FDF delay time results of case 1: 20 SLPM, Eq 1.0

Fig. 3.16 presents local FDF gain results of case 3. For higher fuel flow rate cases, linear response of the flame retained up to the middle part of the flame and nonlinearity tended to appear from the flame tip region. Phase and delay time trends were equivalent to the results of case 1, lower fuel flow rate case.

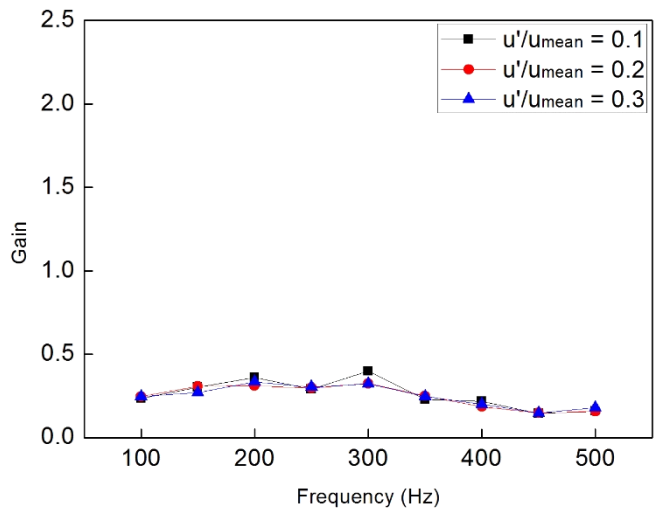

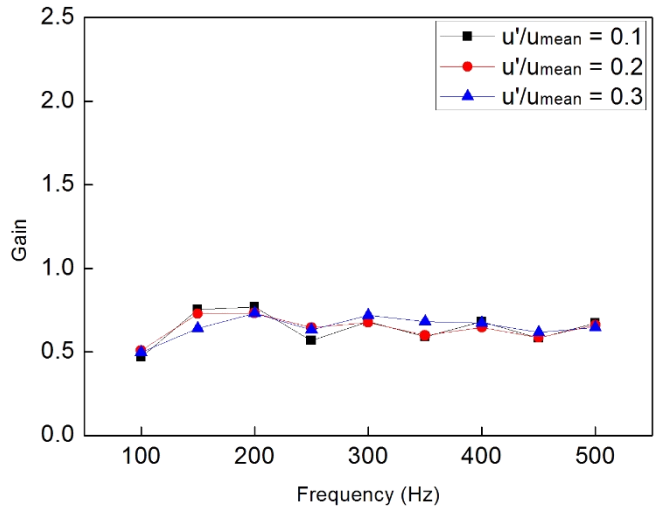

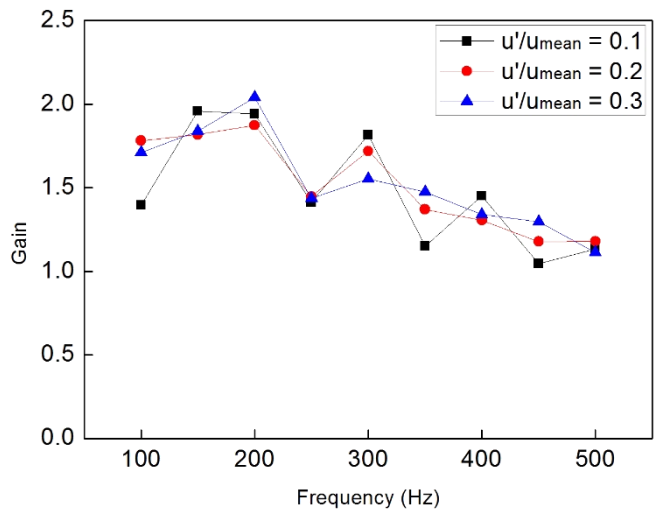

Fig. 3.16 Local FDF gain results of case 3: 45 SLPM, Eq 1.25 (in order of flame base, middle, and tip from the top)

3.3.2. Effect of Flame Length

As the nonlinearity of the flame response was largest at the flame tip, local FDF gain results of flame tip were investigated (mainly comparison between third graph of Fig. 3.13 and 3.16). To find a specific reason for the tendency, a previous work done by B. Jones et al. is referred. As it is shown in Fig. 3.17, the first dip frequency, frequency where the gain reaches its first minimum value and then increases, is known to be dependent on convection velocity and characteristic flame length scale. If the velocity is the same, then the longer flame length results in higher first dip frequency [19]. This kind of trend was found in local FDF gain result of case 1, at the flame tip.

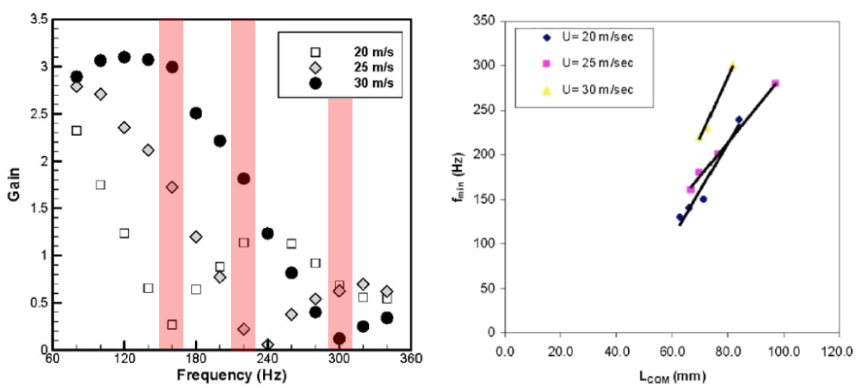

Fig. 3.17 Dependency of first dip frequency on convection velocity and characteristic flame length scale

As it is shown in Fig. 3.18 on the left, for case 1, the first dip frequency was higher at the velocity fluctuation amplitude of 0.3. However, for case 3, the first dip frequency remained the same. This phenomenon was analyzed by utilizing averaged flame length at the flame tip. Fig. 3.19 presents the characteristic flame length of case 1 at the flame tip region. It is clear that higher perturbation magnitude resulted in longer length of the flame. So it is coherent with the previous research that at the same velocity condition, higher first dip frequency was obtained at longer flame length, which in this case, fluctuation amplitude of 0.3. However, for case 3, the flame length did not changed by varied velocity perturbation magnitude, which brought the same first dip frequency value near 250 Hz.

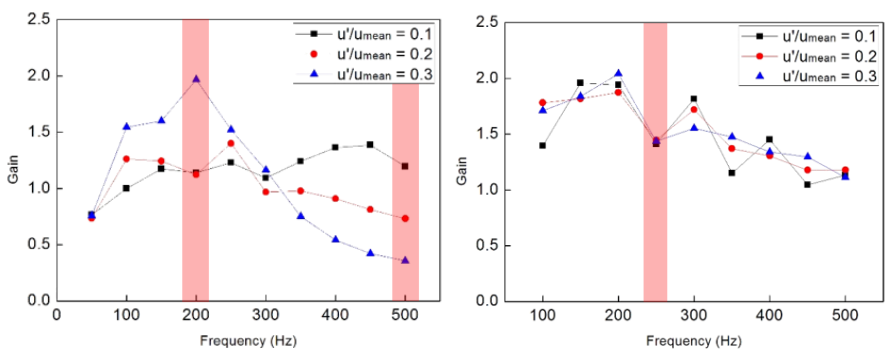

Fig. 3.18 First dip frequency indication on local FDF gain results at the flame tip (left : case 1, right : case 3)

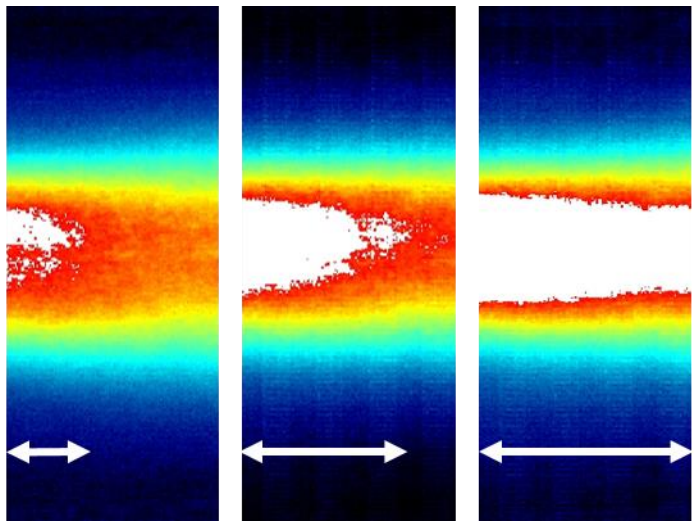

Fig. 3.19 Characteristic flame length of case 1: 20 SLPM, Eq 1.0, at the flame tip

(in order of $u'/\bar{u} = 0.1$, $u'/\bar{u} = 0.2$, and $u'/\bar{u} = 0.3$ from the left)

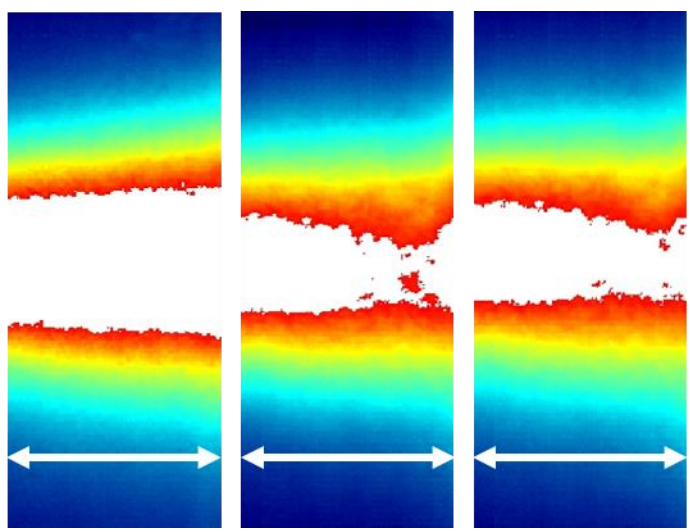

Fig. 3.20 Characteristic flame length of case 3: 45 SLPM, Eq 1.25, at the flame tip

(in order of $u'/\bar{u} = 0.1$, $u'/\bar{u} = 0.2$, and $u'/\bar{u} = 0.3$ from the left)

CHAPTER 4

CONCLUSION

In this particular study, local FTF and FDF were measured by using OH* chemiluminescence images and the results were analyzed by experimental approach in a model rocket combustor. As a result, first of all, global FDF did not have significant difference by various velocity fluctuation amplitudes. Secondly, local heat release rate fluctuation increased towards the flame tip, which had effect on local FTF gain. This was found to be the consequence of flow-flame interaction, which was proved by PIV measurement. Thirdly, through local FDF results, it can be said that nonlinearity of the flame response increased towards the downstream. Also, higher flow rate delayed the nonlinear response of the flame to the tip. In addition, tendency of local FDF flame tip gain results were related to first dip frequency, which depended on characteristic flame length.

Considering the results mentioned above, acoustically non-compact flame shows distinct responses in various regions, which makes spatial analysis such as local FDF, an important factor to predict combustion instability.

REFERENCES

[1] C. H. Kim et al., “Development Trend of Korean Staged Combustion Cycle Rocket Engine,” *Journal of the Korean Society of Propulsion Engineers*, 2018.

[2] M. Sippel et al., “Staged Combustion Cycle Rocket Engine Design Trade-Offs for Future Advanced Passenger Transport,” *Space Propulsion 2012*, 2012.

[3] J. Emdee, “Launch Vehicle Propulsion,” *Crosslink*, 2004.

[4] A. Belluscio, “SpaceX Advances Drive for Mars Rocket via Raptor Power,” *NASAspaceflight.com*, 2014.

[5] T. Lieuwen, “Unsteady Combustor Physics,” *Cambridge University Press*, 2012.

[6] R. Balachandran et al., “Experimental Investigation of the Nonlinear Response of Turbulent Premixed Flames to Imposed Inlet Velocity Oscillations,” *Combustion and Flame*, 2005.

[7] B. D. Bellows et al., “Flame Transfer Function Saturation Mechanisms in a Swirl-Stabilized Combustor,” *Journal of Propulsion and Power*, 2006.

[8] C. Kulsheimer et al., “Combustion Dynamics of Turbulent Swirling Flames,” *Combustion and Flame*, 2002.

[9] C. A. Armitage et al., “Investigation of the Nonlinear Response of Turbulent Premixed Flames to Imposed Inlet Velocity Oscillations,” *Combustion and Flame*, 2006.

[10] T. Schuller et al., “Modeling Tools for the Prediction of Premixed Flame Transfer Functions,” *Proceedings of the Combustion Institute*, 2002.

[11] S. H. Preetham et al., “Response of Turbulent Premixed Flames to Harmonic Acoustic Forcing,” *Proceedings of the Combustion Institute*, 2007.

[12] T. Schuller et al., “A Unified Model for the Prediction of Laminar Flame Transfer Functions: Comparisons Between Conical and V-Flame Dynamics,” *Combustion and Flame*, 2003.

[13] S. Ducruix et al., “Theoretical and Experimental Determinations of the Transfer Function of a Laminar Premixed Flame,” *Proceedings of the Combustion Institute*, 2000.

[14] H. J. Krediet et al., “Identification of the Flame Describing Function of a Premixed Swirl Flame from LES,” *Combustion Science and Technology*, 2012.

[15] F. Boudy et al., “The Flame Describing Function (FDF) Unified Framework for Combustion Instability Analysis : Progress and Limitations,” *International Summer School and Workshop on Non-Normal and Nonlinear Effects in Aero- and Thermoacoustics*, 2013.

[16] J. Lux et al., “Flame Stabilization in High-Pressure Liquid Oxygen/Methane Rocket Engine Combustion,” *Journal of Propulsion and Power*, 2009.

[17] T. S. Cheng et al., “Chemiluminescence Measurements of Local Equivalence Ratio in a Partially Premixed Flame,” *Combustion Science and Technology*, 2006.

[18] K. T. Kim et al., “Spatially Distributed Flame Transfer Functions for Predicting Combustion Dynamics in Lean Premixed Gas Turbine Combustors,” *Combustion and Flame*, 2010.

[19] B. Jones et al., “Flame Response Mechanisms Due to Velocity Perturbations in a Lean Premixed Gas Turbine Combustor,” *Journal of Engineering for Gas Turbines and Power*, 2011.

초 록

액체 로켓 엔진 개발에 있어 다단 연소 사이클 방식으로의 전환이 이루어지고 있으며, 그 중에서도 전 유량 다단 연소 사이클은 긴 엔진 수명과 보다 높은 신뢰성을 가지고 있기에 차세대 로켓 엔진에 적합하다고 할 수 있다. 이러한 엔진 개발에 있어 연소불안정 현상은 연소 효율 저감과 연소실의 파괴로 이어질 수 있기 때문에 이를 예방하기 위한 연구가 필수적이다.

본 연구의 목적은 로켓 연소와 같이 화염이 길이 방향으로 길 경우에는 공간적인 분석이 중요하다는 것을 인지하고, 기존의 화염전달함수와 화염묘사함수에 대하여 화염의 자발광 이미지를 이용하여 국부적으로 구하여 보는 것이다. 또한 이렇게 구해진 국부 화염전달함수와 화염묘사함수에 대하여 실험적인 접근 방법으로 해석해보려는 시도를 하였다.

그 결과, 화염의 열 방출량 섭동은 화염의 끝 부분으로 갈수록 증가하였고, 이는 국부 화염전달함수와 화염묘사함수의 gain에 영향을 미쳤다. 이는 유동과 화염의 상호작용에 의하여 발생한 현상이라고 밝힐

수 있었다. 또한, 국부 화염묘사함수 계측을 통하여 화염의 끝 부분으로 갈수록 화염의 비선형적 응답특성이 강해지는 것을 알 수 있었고, 국부 화염묘사함수의 gain 특성은 화염의 특성 길이와 연관이 있다는 것을 확인하였다. 이러한 결과들을 바탕으로 로켓 화염과 같이 길이 방향으로 긴 화염의 경우에는 연소불안정을 예측하기 위해 사용되는 화염전달함수 및 화염묘사함수를 국부적으로 구하여 이를 이용하는 것이 화염의 반응을 더 잘 반영할 수 있다고 할 수 있다.

주요어 : 연소불안정, 국부 화염묘사함수, 국부 화염전달함수, 국부 열방출량, 모델 로켓 연소기, 스월-제트 동축형 분사기, 속도 섭동, 화염 길이

학 번 : 2016-20729